

Structural, optical and dielectric properties of Zn-doped NiO thin films synthesized via sol-gel route

S. Benhamida^{a,*}, M. Gouamid^b, S. Tlili^a, A. Khenblouche^c, K. Charradi^d

^a*Univ. Ouargla, Fac. des Mathématiques et des Sciences de la Matière, Lab. Rayonnement et Plasmas et Physique de Surface, Ouargla 30 000, Algeria*

^b*Department of Chemistry, Faculty of Mathematics & Material Sciences, University of Ouargla, Ouargla, Algeria*

^c*Laboratory of New and Renewable Energy in Arid Zones – LENREZA, University of Ouargla, Ouargla, Algeria*

^d*Laboratory of Nanomaterials and Systems for Renewable Energies – LaNSER, Research and Technology Center of Energy, Techno-park Borj-Cedria, Hammam-Lif, Tunis, Tunisia*

In this study, pure and Zn-doped nickel oxide thin films have been prepared on glass slides using the sol-gel spin coating process. The effects of Zn doping level concentration (0, 1, 3, and 5%) on structural, morphological, optical, and dielectric properties were studied. The X-ray diffraction patterns revealed that all synthesized films are polycrystalline and correspond to the cubic crystal structure with predominant orientation along the (200) plane. Besides, it was found that with the increase of Zn doping concentration, a variation in the values of several structural parameters such as the crystallite size, the lattice constant, and the strain was observed. The surface morphology examined by scanning electron microscope (SEM) reveals that the deposited film becomes dense, smooth, and agglomeration is increased as the Zn doping level increases. FT-IR analyses confirm the existence of Ni-O bonds. From UV-vis measurements, it is found that all samples exhibit highly optical transmission, more than 80% in the visible region, while the optical band gap values vary from 3.76 to 3.93eV as a function of Zn doping content. Further, the refractive index, extinction coefficient, and dielectric constants were also determined.

(Received December 31, 2020; Accepted April 6, 2021)

Keywords: Thin films, NiO, Zn doping, sol-gel route, X-ray diffraction, Optical properties

1. Introduction

Nickel oxide (NiO) is one of few p-type metal oxide semiconductors that received extensive attention for decades due to its specific physical and chemical properties such as highest exciton binding energy (110 meV), wide direct band gap (4.0 eV), low materials cost, excellent chemical and thermal stability [1-3]. NiO thin films have been advantageous for diverse potential applications such as magnetic material, transparent electronics, heterojunction solar cells, smart windows, and gas sensors. [4-7]. Doping is a useful technique used to control and enhance optoelectronic properties to produce new materials for technological applications. However, different reports have been studied extensively on ion doping with various transition metals (Li, Al, Cu, Co) on NiO properties [8-11]. Recently, few reports focused on the synthesis and deposition of zinc doped NiO thin layer. Besides, doping with Zn ion can change the optoelectronic behavior of NiO by altering the band structure [12-14]. In this regard, doping with Zn elements in NiO film has been proposed in this study. Various deposition techniques are currently available to fabricate NiO thin films, including thermal oxidation, electron beam evaporation, sol-gel, chemical bath deposition, and spray nebulizer [15-19]. Compared with previous techniques, the sol-gel spin coating process can be considered a simple and cost-effective method involving low deposition temperature, good control over the coating process, and a large

* Corresponding author: benhamidas9@gmail.com

deposition area [20]. In this paper, pure and Zn-doped NiO films were synthesized via sol-gel spin coating process on glass substrates, the effect of Zn doping level on structural, surface morphology optical, and dielectric properties were investigated.

2. Materials and preparation

In this work, pure and Zn-doped NiO (NiO: Zn) thin films were synthesized using a sol-gel spin coating process on to glass substrate. Nickel (II) acetate [$\text{Ni}(\text{OCOCH}_3)_2 \cdot 4\text{H}_2\text{O}$] (98%, Sigma Aldrich) was used as a starting material. Zinc acetate dehydrates [$\text{Zn}(\text{CH}_3\text{COO})_2 \cdot 2\text{H}_2\text{O}$] (98%, Sigma Aldrich), 2-Methoxyethanol [$\text{C}_3\text{H}_8\text{O}_2$] (99.8%, Sigma Aldrich), and Monoethanolamine [$\text{C}_2\text{H}_7\text{NO}$, MEA] (99%, Sigma Aldrich) was used as a dopant, solvent, and stabilizer, respectively. For the preparation of the pure NiO precursor solution, nickel (II) acetate was initially added in 2-Methoxyethanol to obtain a final concentration of 0.5 M. The obtained solution was stirred slowly for 1 h at 60°C ; at that moment, a few drops of MEA was added to achieve a transparent and homogeneous green solution. Before the deposition process, the glass slides were consecutively cleaned with acetone, ethanol, and double-distilled water for 5 min. The obtained mixture solution was dropped on glass slides using a spin coater device with the rotation rate fixed at 3000 rpm for 30 s. The as-deposited NiO films were dried at 100°C for about 5 min to remove organic contaminations. The last process was repeated four times. For the preparation of Zn doped NiO films, the same procedure was repeated from solutions prepared by adding zinc acetate to the mixture solution with different molar ratios ($[\text{Zn}]/[\text{Ni}]$) were 0%, 1%, 3%, and 5%. Finally, all deposited films were annealed at 350°C in the air for 2 h.

3. Characterization methods

The structural properties of all prepared samples were explored using X-ray diffraction (BRUKER-AXS type D8) equipped with X'Pert High Score under Cu $K\alpha$ radiation source ($\lambda=1.5406\text{\AA}$) operating at 40 kV and 30 mA in the range of the diffraction angles (2θ) between 30° and 60° . Scanning electron microscope (SEM; Jeol JSM 6360LV) was carried out for the films surface morphology analysis. The functional group of the achieved films was characterized using Fourier transformed infrared spectroscopy (FTIR -Perkin Elmer Spectrum 1000) in the range of $400\text{-}4000\text{ cm}^{-1}$. The optical studies were performed using Agilent Cary 5000 UV-Vis-NIR spectrophotometer in the wavelength range 300-900 nm. However, the film thickness (d) was calculated via the weight difference method, taking into account the bulk NiO material density.

4. Results and discussion

4.1. Structural properties

Fig. 1 demonstrates the X-ray diffraction (XRD) patterns of the pure NiO and Zn-doped NiO films with various Zn concentrations. The XRD results indicate two prominent diffraction peaks located at $2\theta = 37.38^\circ$ and 43.30° , corresponding to the (111) and (200) planes. From the XRD patterns, it is observed that all the films are polycrystalline, and the intensity of the (200) diffraction peak was observed higher compared with other peaks indicating the preferred orientation. XRD analysis indicates that the deposited films indexed to the face-centered cubic of the NiO phases and excellently coincides with the standard NiO of JCPDS card N $^\circ$ 47-1049 [21]. It was found that no phase or impurities related to Zn or its oxides can be detected from XRD data, which proves that Zn ions uniformly incorporate into NiO lattice.

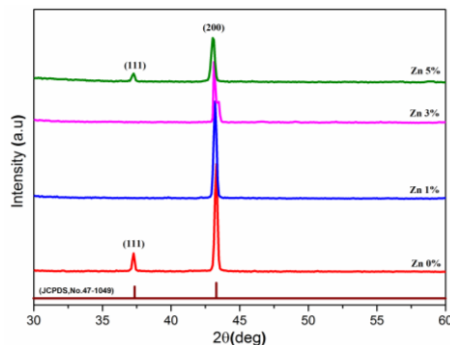


Fig. 1. X-ray diffraction pattern of pure and Zn-doped NiO thin films.

Moreover, the intensity of diffraction (200) peak is gradually reduced as Zn doping concentrations increase; this may be probably due to the diminution of crystallinity of (NiO: Zn) films [22]. Also, it is observed that the diffraction peaks of doped NiO films shifted slightly toward the lower 2θ angle as compared to the pure NiO sample, as seen in Fig. 2. This behavior was attributed to the variation of ionic radii of Zn^{+2} (0.74 Å) and Ni^{+2} (0.69 Å), which leads to the substitution of Ni ions by Zn ions in the NiO lattice; similar results are also reported in the literature [23, 24].

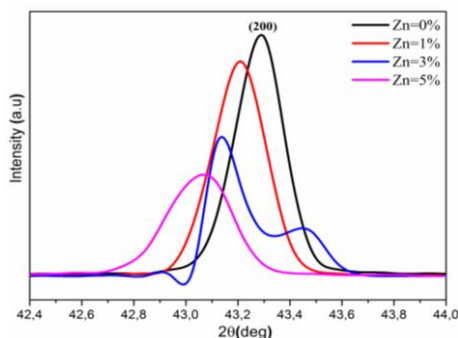


Fig. 2. X-ray patterns of pure and Zn-doped NiO thin films in the range 2θ (42.4° – 44.0°) corresponding to the (200) plane.

The mean crystallite size (G) of pure NiO and Zn doped NiO films was determined using the Debye-Scherrer equation given below [18]:

$$G = \frac{0.9\lambda}{\beta \cos \theta} \quad (1)$$

where β is the full width at half-maximum intensity ($FWHM$), λ is the wavelength of the incident X-ray (1.54056 Å), and θ is the Bragg angle at (200) plane.

Since the prepared films are the cubic structure, the lattice constants a of NiO films can be estimated using the relation [4]:

$$a = d_{hkl} \cdot \sqrt{(h^2 + k^2 + l^2)} \quad (2)$$

where (h , k , l) is the miller indices of a related plane, and d_{hkl} is the interplanar spacing.

The mean strain ϵ was calculated by using the well known Scherrer's relation given below [18]:

$$\varepsilon = \left(\frac{a - a_0}{a_0} \right) \times 100\% \quad (3)$$

where a is the calculated lattice constant of NiO thin films and a_0 the theoretical lattice constant of bulk NiO material ($a_0 = 4.1769 \text{ \AA}$) corresponding to the standard card (JCPDS, No. 47-1049). Values of different structural parameters such as mean crystallite size, the lattice constant, and mean strain at different Zn concentrations are illustrated in Table.1. As seen in Fig. 3, the crystallite size of the prepared films decreased from 18.79 nm for pure NiO and 13.01, 11.58, and 9.84 nm for the Zn doped NiO film with Zn = 1 %, 3%, and 5 %, respectively. The decrease in the crystallite size is mainly due to the substitution of Ni^{2+} ions with Zn^{2+} ions in the NiO lattice. As a result, the crystallinity of the NiO material degrades. On the other hand, the lattice constant was increased from 4.192 to 4.274 \AA with increases of Zn doping level from 0 to 5%. The increase in lattice constant could be attributed to the substitution of Zn^{2+} ion with Ni^{2+} ion in the NiO lattice; this behavior induces the increase in the length of a-axis lattice constant as the Zn concentration is increased [25]. It can be seen from Table.1 that the mean strain ε is increased from 0.3615 to 2.3246% as the Zn doping level increases from 0 to 5%. The increase in the mean strain is related directly to the variation of crystallite size, which leads to enhancement of defects and internal strain in NiO host lattice, as reported in the previous discussion [26].

Table 1. Values of Bragg angle 2θ , lattice constants a , crystallite size G , and mean strain ε for the (200) plane of NiO thin films as a function to the zinc concentration.

| Zn Concentration (%) | 2θ (deg) | Lattice constant (\AA) | | Crystallite size G (nm) | Mean strain ε (%) |
|----------------------|-----------------|-----------------------------------|----------------------|---------------------------|-------------------------------|
| | | a | $\Delta a = a - a_0$ | | |
| 0 | 43,27 | 4,192 | 0,0151 | 18,79 | 0,3615 |
| 1 | 43,21 | 4,210 | 0,0331 | 13,01 | 0,7924 |
| 3 | 43,15 | 4,232 | 0,0551 | 11,58 | 1,3191 |
| 5 | 43,07 | 4,274 | 0,0971 | 9,84 | 2,3246 |

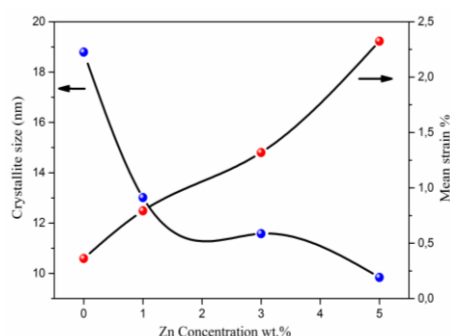


Fig. 3. Variation of crystallite size and mean strain of NiO thin films as a function of Zn doping concentration.

4.2. Surface morphology analysis

The surface morphology of pure NiO and NiO: Zn (0 to 5 wt.%) doped thin films were done by scanning electron microscopy (SEM) are illustrated in Fig. 4. From the naked eye, it can be observed that all deposited layers have a similar surface with dense and good adherence to the glass slides. From the SEM images (Fig. 4 (a)), the pure NiO sample's surface morphology shows that the film is smooth, with uniform growth, and illustrates a homogeneous surface. In Fig. 4 (b), the SEM image demonstrates that the films have the same morphology as the undoped NiO film, indicating that doping with Zn (at 1wt.%) does not make a noticeable change in the morphology. As the Zn content increases from 3 to 5 %, the surface morphology of the film becomes rougher,

and agglomeration of particles with the formation of some microplates dispersed throughout the substrate's surface is observed from Fig. 4 (c, d). A similar result was also reported by Kate et al. [27]. As a result, the synthesized films surface morphology is highly influenced by the increase of Zn concentration.

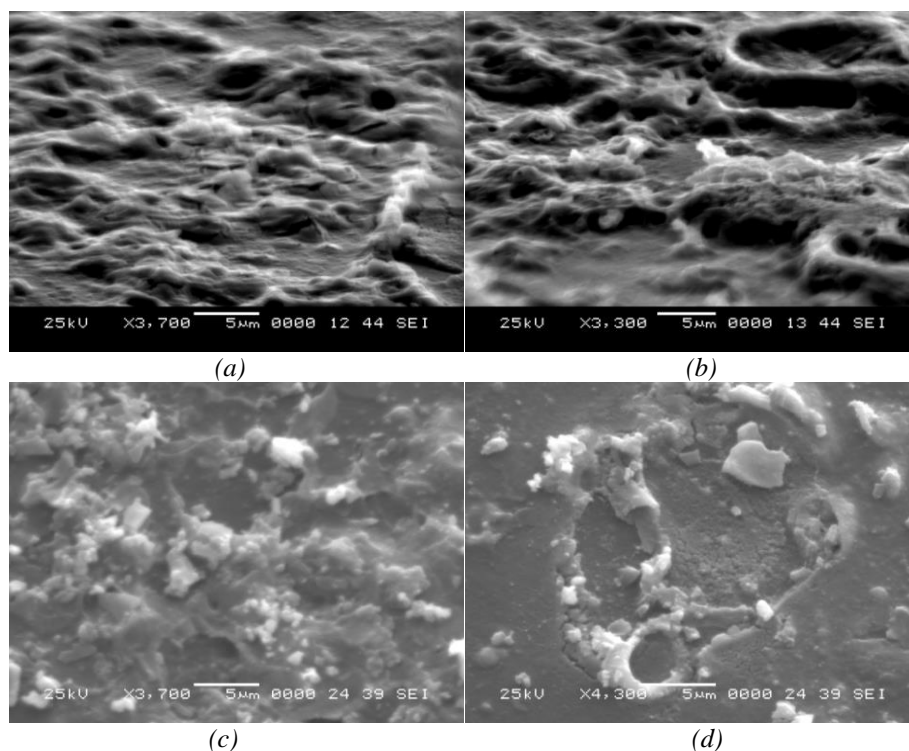


Fig. 4. Surface SEM images of: (a) Zn=0% (b) Zn=1% (c) Zn=3% and (d) Zn=5% of NiO thin films.

4.3. Functional group analysis

To identify the chemical bonding state and confirm the functional groups of the synthesized samples, Fourier transforms infrared spectroscopy (FTIR) was investigated. FTIR spectra of pure NiO and Zn doped NiO thin films recorded from 4000 to 400 cm^{-1} are illustrated in Fig.5. The absorption band is located at 3693 cm^{-1} , related to the O-H stretching vibrations [12]. The band centered at 2945 cm^{-1} referred to the C-H vibrations mode [28]. The broad absorption band located at 1845 cm^{-1} may be related to the C=H stretching vibrations mode [29]. The band at 1170 cm^{-1} represents the C-O vibrations [30]. Two absorption bands around 435 and 615 cm^{-1} are observed, which corresponds to the stretching vibrations of Ni-O bonds; these results prove the presence of NiO material [25]. The spectra show that the NiO bands (435 and 615 cm^{-1}) are shifted to the lower wavenumber region as the Zn concentration level increases; this indicates the incorporation of Zn ion inside the NiO lattice.

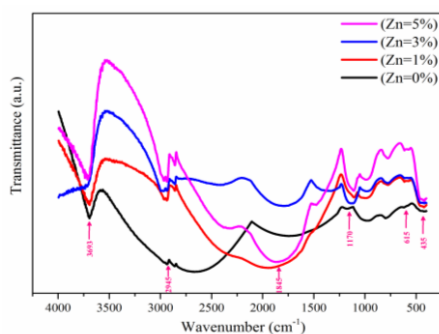


Fig. 5. FT-IR spectra of pure and Zn-doped NiO thin films.

4.4. Optical properties

The optical transmittance spectra of the prepared films were registered in the range between 300 and 900 nm and illustrated in Fig. 6. From the figure, all deposited films exhibited high optical Transparency of about 80% over the visible region. Besides, the absorption edge gradually shifts toward the shorter wavelength region (blue shift) as the Zn doping level increases in the range below 380nm. This shift may be referred to the increment in grain size, the presence of crystal defects, and surface roughness of the films, as it was established by XRD analysis and SEM images.

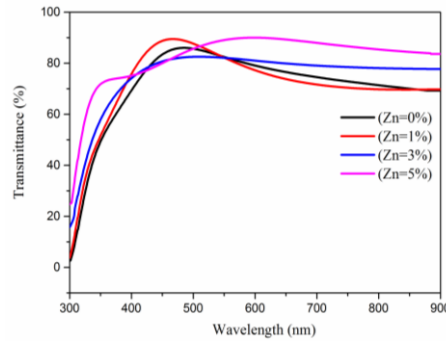


Fig. 6. Transmittance spectra of pure and Zn-doped NiO thin films.

The absorption coefficient (α) was estimated from transmittance T and thickness d with respect to the expression below [19]:

$$\alpha = \ln\left(\frac{1}{T}\right)/d \quad (5)$$

We can estimate the value of the bandgap energy (E_g) of all deposited films from the absorbance using the Tauc's relationship [3]:

$$(\alpha h\nu) = B(h\nu - E_g)^{\frac{1}{2}} \quad (6)$$

where B , α , and $h\nu$ are constant, the absorption coefficient, and photon energy, respectively. The values of gap energy (E_g) can be calculated by drawing $(\alpha h\nu)^2$ versus photon energy ($h\nu$), as presented in Fig.7. The calculated (E_g) values of the deposited films are recorded in Table. 2. As observed in Table.2, the E_g value of pure NiO films was estimated to be 3.76 eV, which is in good converging with earlier reports [26]. Therefore, the E_g values vary between 3.74 and 3.93 eV as Zn doping content increases from 1% to 5 %. This increase in the optical band gap may be due to the crystallite size change, lattice defects, and impurities due to the incorporation of Zn dopant in the NiO lattice [23].

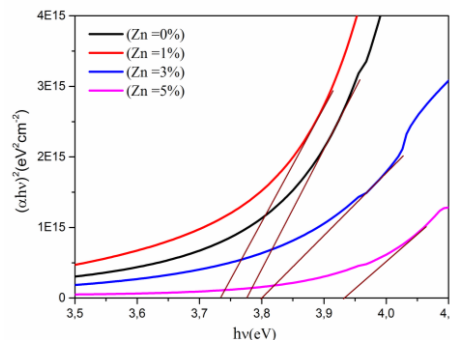


Fig. 7. Plot of $(\alpha h\nu)^2$ versus photon energy ($h\nu$) of pure and Zn-doped NiO thin films.

The Urbach tail (E_u) presents the degree of structural disorder of the films. E_u values can be determined by the equation below [21]:

$$\alpha = \alpha_0 \exp\left(\frac{h\nu}{E_u}\right) \quad (7)$$

where α_0 , E_u and $h\nu$ are constant, the Urbach energy, and the photon frequency, respectively. E_u values can be evaluated from the $\ln(\alpha)$ plot against ($h\nu$) as shown in Fig.8. E_u values have been estimated, and the results are listed in Table. 2. It has been observed that the E_u values decrease from 324 to 298 meV as the Zn doping level increases. This behavior depends on the defects, internal strain and disorder in the NiO lattice [18]. We can also observe from Table 2 that Urbach energy inversely changes with the gap energy as Zn doping concentration increases.

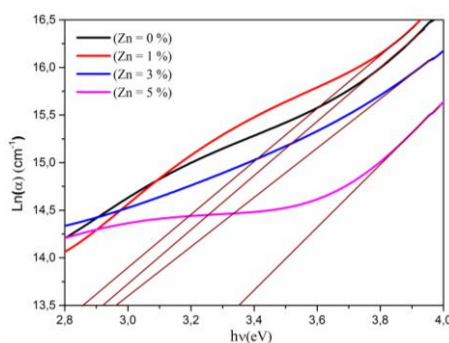


Fig. 8. Plot of $\ln(\alpha)$ versus photon energy ($h\nu$) of pure and Zn-doped NiO thin films.

Optical dispersion parameter such as the index of refraction (n) and extinction coefficient (k) plays a significant function in the optoelectronic and transparent electrode applications.

The values of (n) and (k) of the prepared NiO films were determined by the following equations [31]:

$$n = \left(\frac{1-R}{1+R}\right) + \sqrt{\frac{4R}{(1-R)^2} - k^2} \quad (8)$$

and

$$k = \frac{\alpha\lambda}{4\pi} \quad (9)$$

where (λ), (R), (α), and (k) are the wavelength, the reflectance, the absorption coefficient, and the extinction coefficient, respectively.

Fig. 9 and Fig. 10, demonstrated the variation of (n) and (k), with the wavelength for the prepared NiO films, respectively. The values of (n) and (k) at wavelength 550nm of all films are shown in Table.2. It is observed from Table. 2 that the refractive index values have been increased gradually from 2.71 to 2.89 as the Zn doping level increased from 0 to 5%. The increment in the (n) values may be due to the improvement in crystallinity and packing density of the NiO films as Zn doping concentration increases. The same results were obtained with other research paper [32].

However, the value of the extinction coefficient was found to be varied between 0.010 and 0.018, with increases of Zn doping. The little values of k indicated that the prepared films have high optical transparency and enhanced the surface homogeneity [31, 33].

Table 2. Values of thickness d , band gap energy E_g , Urbach energy E_u , refractive index n and extinction coefficient k of NiO thin films as a function to the zinc concentration.

| Zn concentration % | Thickness d (nm) | Optical gap energy E_g (eV) | Urbach energy E_u (meV) | Refractive index n (550nm) | Extinction coefficient k (550nm) |
|--------------------|--------------------|-------------------------------|---------------------------|------------------------------|------------------------------------|
| 0 | 133 | 3.76 | 324 | 2.71 | 0,010 |
| 1 | 100 | 3.74 | 349 | 2.82 | 0,008 |
| 3 | 131 | 3.80 | 337 | 2.86 | 0,013 |
| 5 | 157 | 3.93 | 298 | 2.89 | 0,018 |

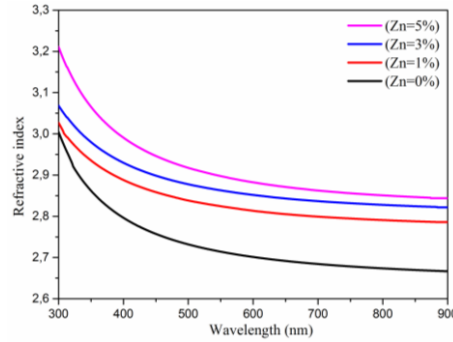


Fig. 9. Refractive index (n) of pure and Zn-doped NiO thin films as a function of wavelength (λ).

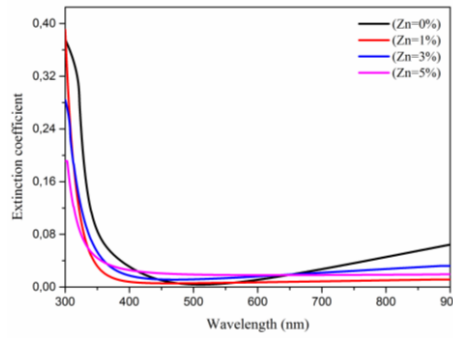


Fig. 10. Extinction coefficient (k) of pure and Zn-doped NiO thin films as a function of wavelength (λ).

4.5. Dielectric properties

Dielectric properties of undoped and Zn-doped NiO can be obtained easily according to (n) and (k), the real (ε_1) and imaginary part (ε_2) of the dielectric constants of the prepared films were calculated via the equations below [34]:

$$\varepsilon_1 = n^2 - k^2 \quad (10)$$

and

$$\varepsilon_2 = 2n \cdot k \quad (11)$$

The variation of ε_1 and ε_2 upon the wavelength λ for NiO films are shown in Fig. 11 and Fig. 12, respectively. The real part ε_1 of all films was found to be enhanced brusquely with the increase of photon energy; however, the imaginary part ε_2 is approximately constant in the lower energy region and increases rapidly starting from 348nm.

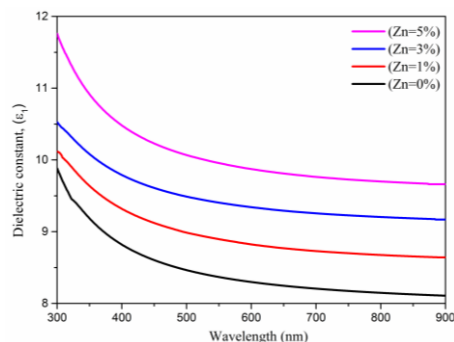


Fig. 11. The variation of the real dielectric constant (ϵ_1) of pure and Zn-doped NiO thin films as a function of wavelength (λ).

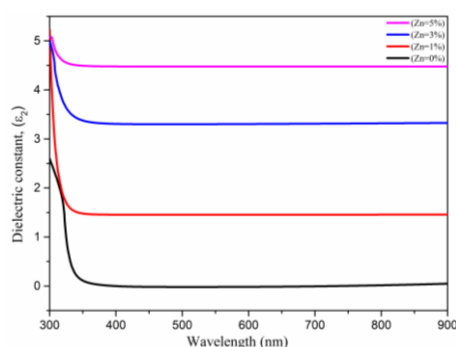


Fig. 12. The variation of *b* Imaginary dielectric constant (ϵ_2) of pure and Zn-doped NiO thin films as a function of wavelength (λ).

5. Conclusion

In summary, undoped and Zn-doped NiO films were synthesized successfully using the sol-gel spin coating route on a glass slide. The influence of Zn doping concentration varied from 0% to 5% on their structural, morphological, optical, and dielectric properties of NiO thin films has been investigated. XRD analyses revealed that all prepared samples crystallized in the cubic phase with (200) plane as a preferential orientation; however, the grain size was in the range 9.84–18.79 nm. SEM micrographs showed that the Zn-doped NiO samples become dense, rougher, and agglomeration increased with Zn concentration. FTIR measurements affirm the existence of bonds related to the Ni-O structure.

The optical transmission of all films was over 80% in the visible wavelength region, whereas the gap energy was increased from 3.76 to 3.93 eV as the Zn doping level increases. Furthermore, the refractive index of the films was found to vary strongly upon Zn content. The high quality of the prepared films is confirmed by the low value of the extinction coefficient. These results suggest that present films may act as potential candidates for the fabrication and design of modern optoelectronic devices and solar cells.

References

- [1] T. P. Mokoena, K. T. Hillie, H. C. Swart, N. Leshabane, J. Tshilongo, D. E. Motaung, *Materials Chemistry and Physics*, **253**, 123316 (2020).
- [2] W. Xu, H. Li, J-B. Xu, L. Wang, *ACS Appl. Mater. Interfaces* **10**(31), 25878 (2018).
- [3] M. A. Hameed Omar, A. Ali Sarmed, S.M. Al-Awadi, *Optik* **206**, 164352 (2020).
- [4] Adiba, V. Pandey, S. Munjal, T. Ahmad, *Materials Today: Proceedings* **26**, 3116 (2020).

- [5] J. K. Kim, D. N. Nguyen, J. H. Lee, S. Kang, Y. Kim, S. S. Kim, H. K. Kim, *Journal of Alloys and Compounds* **818**, 152887 (2020).
- [6] K. H. Wang, M. Yoshida, H. Ikeuchi, G. Watanabe, Y. L. Lee, C. C. Hu, T. Kawai, *Journal of the Taiwan Institute of Chemical Engineers* **110**, 34 (2020).
- [7] U. T. Nakate, R. Ahmad, P. Patil, Y. T. Yu, Y. B. Hahn; *Applied Surface Science* **506**, 144971 (2020).
- [8] J. Chen, Y. Wu, K. Zhu, F. Sun, C. Guo, X. Wu, G. Cheng, R. Zheng, *Electrochimica Acta* **316**, 133 (2019).
- [9] V. Kampitakis, E. Gagaoudakis, D. Zappa, E. Comini, E. Aperathitis, A. Kostopoulos, G. Kiriakidis, V. Binas, *Materials Science in Semiconductor Processing* **115**, 105149 (2020).
- [10] T. Ç. Taşdemirci, *Chemical Physics Letters* **738**, 136884 (2020).
- [11] R. S. Kate, S. C. Bulakhe, R. J. Deokate, *Optical and Quantum Electronics* **51**(10), 319 (2019).
- [12] S. Parwani, P. Dubey, R. C. Dixit, N. Kaurav, *AIP Conference Proceedings* **2100**, 020092 (2019).
- [13] K. H. Kim, M. Kahuku, Y. Abe, M. Kawamura, T. Kiba, *Int. J. Electrochem. Sci.* **15**, 4065 (2020).
- [14] X. Jiang, Z. Wang, Q. Deng, F. Zhang, F. You, C. Yao, *Eur. J. Inorg. Chem.* **39**, 4345 (2018).
- [15] F. Hajakbari, *Journal of Nanostructure in Chemistry* **10**, 97 (2020).
- [16] A. K. Mahmud Hasan, K. Sobayel, I. Raifuku, Y. Ishikawa, Md. Shahiduzzaman, M. Nour, H. Sindi, H. Moria, M. Rawa, K. Sopian, N. Amin, Md. Akhtaruzzaman, *Results in Physics* **17**, 103122 (2020).
- [17] J. Zhao, A. Ho-Baillie, S. P. Bremner, *Journal of Vacuum Science & Technology B* **38**, 014013 (2020).
- [18] S. Benhamida, B. Benhaoua, R. Barir, A. Rahal, A. Benhaoua, *Journal of nano- and electronic physics* **9**, 03001(2017).
- [19] N. R. Aswathy, J. Varghese, R. Vinodkumar, *Journal of Materials Science: Materials in Electronics* (2020).
- [20] V. Ganesha, L. Harithab, M. A. Manthrammel, M. Shkir, S. AlFaify, *Physica B: Condensed Matter* **582**, 411955 (2020).
- [21] Rafia Barir, B. Benhaoua, S. Benhamida, A. Rahal, T. Sahraoui, R. Gheriani, *Journal of Nanomaterials* **10**, 5204639 (2017).
- [22] M. Abdur Rahman, R. Radhakrishnan, R. Gopalakrishnan, *Journal of Alloys and Compounds* **742**, 421 (2018).
- [23] J. Al Boukhari, L. Zeidan, A. Khalaf, R. Awad, *Chemical Physics* **516**, 116 (2019).
- [24] B. J. Rani, G. Ravi, R. Yuvakkumar, S. Ravichandran, F. Ameen, A. Al-Sabri, *J. Sol-Gel Sci. Technol.* **89**(2), 500 (2019).
- [25] S. Dewan, M. Tomar, R. P. Tandon, V. Gupta, *journal of applied physics* **121**, 215307 (2017).
- [26] C. Thangamani, K. Pushpanathan, *J. Chem. Pharm. Res.* **8**, 749 (2016).
- [27] R. S. Kate, S. C. Bulakhe, R. J. Deokate, *Journal of Electronic Materials* **48**, 3220 (2019).
- [28] A. B. Gemta, B. Bekele, A. R. Chandra Reddy, *Journal of Nanotechnology and Materials Science* **5**(1), 44 (2018).
- [29] S. Husain, F. Rahman N. Ali, P. A. Alvi, *Journal of Optoelectronics Engineering* **1**, 28 (2013).
- [30] M. N. Siddique, T. Ali, A. Ahmed, P. Tripathi, *Nano-Structures & Nano-Objects* **16**, 156 (2018).
- [31] K. S. Usha, R. Sivakumar C. Sanjeeviraja, *Journal of Applied Physics* **114**, 123501 (2013).
- [32] M. Anitha, L. Amalraj, N. Anitha, *Applied Physics A* **123** (12), 764 (2017).
- [33] I. M. El Radaf, A. H. Talaat, G.M. El komy, T.M. Dahy, *Ceramics International* **45** (3), 3072 (2019).
- [34] M. I. Mohammed, S. S. Fouad, N. Mehta, *Journal of Materials Science: Materials in Electronics* **29**(21), 18271 (2018).